Turbulent flow over a flexible wall undergoing a streamwise travelling wave motion

By L I A N S H E N, X I A N G Z H A N G, D I C K K. P. Y U E†
AND M I C H A E L S. T R I A N T A F Y L L O U

Department of Ocean Engineering, Massachusetts Institute of Technology, Cambridge, MA 02139, USA

Direct numerical simulation is used to study the turbulent flow over a smooth wavy wall undergoing transverse motion in the form of a streamwise travelling wave. The Reynolds number based on the mean velocity U of the external flow and wall motion wavelength λ is 10 170; the wave steepness is $2\pi a/\lambda = 0.25$ where a is the travelling wave amplitude. A key parameter for this problem is the ratio of the wall motion phase speed c to U, and results are obtained for c/U in the range of -1.0 to 2.0 at 0.2 intervals. For negative c/U, we find that flow separation is enhanced and a large drag force is produced. For positive c/U, the results show that as c/U increases from zero, the separation bubble moves further upstream and away from the wall, and is reduced in strength. Above a threshold value of $c/U \approx 1$, separation is eliminated; and, relative to small- c/U cases, turbulence intensity and turbulent shear stress are reduced significantly. The drag force decreases monotonically as c/U increases while the power required for the transverse motion generally increases for large c/U; the net power input is found to reach a minimum at $c/U \approx 1.2$ (for fixed U). The results obtained in this study provide physical insight into the study of fish-like swimming mechanisms in terms of drag reduction and optimal propulsive efficiency.

1. Introduction

Turbulent flow over a body undergoing transverse flapping in the form of a streamwise-travelling wave is related to fish swimming. It has been hypothesized (e.g. Triantafyllou, Triantafyllou & Yue 2000) that the travelling wave motion contributes to a reduced drag force and increased propulsive efficiency by reducing separation and suppressing turbulence. Taneda & Tomonari (1974) demonstrated experimentally that when the wave phase velocity c is smaller than the external flow velocity U, the boundary layer separates at the back of the wave crest, but when c is larger than U, the boundary layer does not separate. He also observed that the travelling wave motion has a tendency to laminarize the flow and the fluid motion in the wave direction is accelerated. These striking results pose the challenge of obtaining a theoretical understanding, while they provide an opportunity for engineers to achieve turbulence control. Few other publications on turbulence over a travelling wavy wall exist. Benjamin (1959) provided a linear analysis for fixed travelling wavy motion between two fluids. Later Kendall (1970) studied experimentally the effects of a travelling wavy wall for $ka = 0.18$, with k and a the wavenumber and wave amplitude, respectively.

† Author to whom correspondence should be addressed: yue@mit.edu

He observed a decrease in pressure perturbations compared to flow over a fixed wavy wall.

Before considering a wavy wall, we review some results pertaining to flow over a curved surface. Measurements of turbulent boundary layers along a convex surface obtained by So & Mellor (1973) indicated that Reynolds stress was decreased. Experimental work on the boundary layer over a concave surface is not as extensive, but the opposite effect was observed by Eskinazi & Yeh (1956) for a concave surface. The effects of stabilizing or destabilizing forces on the turbulent motion on a curved surface was first discussed by Prandtl (1930). Normal pressure gradients generated by the centrifugal force can suppress surface-normal momentum exchange for convex surfaces. Görtler (1940) observed that at high Reynolds numbers, laminar boundary layer flows over a concave surface develop an alternating sequence of rolling structures under certain conditions. The stability of this flow is qualitatively similar to the Taylor–Görtler inertial instability in rotating fluids. Bradshaw (1969) showed that an analogy between buoyancy-induced instability and curvature-induced instability can be achieved by using the Richardson number. For compressible flow over a curved wall, Rotta (1967) calculated the contribution of the Coriolis force to energy production and found that compressibility enhances the wavy wall effects.

The flow over a fixed wavy surface is subject to the effects of alternating convex and concave curvature. Many experiments have been performed on turbulent flows over a stationary sinusoidally shaped solid surface, including Zilker, Cook & Hanratty (1977), Abrams & Hanratty (1985) and Frederick & Hanratty (1988) for small-amplitude wavy surfaces, Zilker & Hanratty (1979), Kuzan, Hanratty & Adrian (1989) and Hudson, Dykhno & Hanratty (1996) for medium-amplitude surfaces, and Buckles, Hanratty & Adrian (1984) for large-amplitude surfaces. It is found that a wavy surface substantially modifies flat-wall turbulence results such as the law of the wall and turbulence production mechanisms. While a linearized approximation is applicable when the wave amplitude is small, the flow field becomes much more complicated when the wave amplitude is large enough so that separation occurs, and it contains different flow elements including an outer flow, a separated region, an attached boundary layer and a free shear layer. Recently, numerical simulations have been performed for turbulent flows near a fixed wavy surface. The results obtained by Maass & Schumann (1994), De Angelis, Lombardi & Banerjee (1997), Cherukat et al. (1998) and Calhoun & Street (2001) not only confirm the previous experimental measurements, but also add a detailed three-dimensional instantaneous physical picture including the discovery of velocity bursts originating in the separated region, a detailed analysis of the turbulent kinetic energy budget, and elucidation of instantaneous vortex structures.

The travelling wavy wall flow differs from the flow near a fixed wavy wall in that the wall wavy displacements propagate in the streamwise direction. Locally, the wall undergoes an up–down oscillation, which adds complexity to the problem as the boundary layer is displaced non-uniformly. Unlike in the fixed wall case, the wavy surface is no longer a streamline. If viewed in a frame moving with the phase velocity of the waving motion and if the wave amplitude does not vary in space, the wavy surface is still a streamline in that the surface slides non-uniformly in its tangential direction. As a fluid particle moves along the surface, alternating convex and concave curvatures are encountered and the flow is strongly affected by surface-normal pressure gradients and centrifugal forces. The effects of a surface-normal pressure gradient are evident the flow over a rotationally oscillating cylinder, in which case separation can be reduced dramatically as demonstrated by Tokumaru

& Dimotakis (1991). Longuet-Higgins (1969) showed that sinusoidal shear stress is dynamically equivalent to a pressure force on the wave. We emphasize that for the travelling wavy wall, the surface motion is not simply the translation or rotation of a solid body surface, since both the gliding velocity of a fluid particle along the surface and the surface extension or compression are non-uniform. The pressure distribution mechanism over a wavy surface without separation is treated by Miles (1957, 1959) with an inviscid theory. Turbulence reduction through travelling wave actuation, but in the spanwise direction is shown in Du & Karniadakis (2000) and Du, Symeonidis & Karniadakis (2002).

For aquatic animal locomotion, Gray (1936) observed that an actively swimming dolphin only consumes one seventh of the energy needed to tow a rigid body at the same speed, and he suggested that this difference might be explained by the turbulence suppression effects caused by the body motion. Wu (1961) developed a theory for the swimming propulsion mechanism of a plate moving at variable forward speed in an inviscid fluid. Using a laboratory fish-like vehicle, Barrett *et al.* (1999) showed that the power required to propel a swimming body may be smaller than the power needed to tow a straight-rigid body. In order to understand fish swimming propulsion, two interdependent aspects of the problem need to be studied: (i) the nature of the force resisting the motion, and (ii) the mechanisms that lead to the thrust force.

This paper applies direct numerical simulation (DNS) to study the turbulent boundary layer flow over a travelling wavy wall. One of the key issues is the effect of the ratio of the wave motion phase speed to mean velocity c/U on turbulence amplification and suppression. Two aspects of this problem will be discussed: (1) the effects of travelling wave motion on the mean flow field and turbulence fluctuations, and (2) the averaged force and power balance on the body (the wavy wall). The nature of the turbulence modification is examined: whether it varies uniformly with c/U, or displays local minima and maxima of drag force and power consumption.

This paper is organized as follows: the problem definition and numerical method are stated in §2. Section 3 presents results, including mean flow profiles, turbulence statistics, and variation of drag force and power consumption. Section 4 provides a discussion and conclusions.

2. Problem definition and numerical method

### 2.1. *Physical problem and mathematical formulation*

We consider a three-dimensional incompressible turbulent flow over a moving wall undergoing a travelling wave motion. As shown in figure 1, the flow is in the frame (x, y, z) where x, y and z (also denoted as x_1, x_2 and x_3 when tensor notation is used) are streamwise, vertical and spanwise coordinates, respectively. The wall is undergoing a vertical oscillation in the form of a wave travelling in the streamwise direction. The position of the wall is given by

$$y_{\mathrm{w}} = a \sin k(x - ct). \tag{2.1}$$

Here a is the magnitude of the displacement, $k = 2\pi/\lambda$ is the wavenumber with λ the wavelength, c is the phase speed of the wave.

Points on the wall have an up–down oscillation with velocity components given by

$$\left. \begin{aligned} u_{\mathrm{w}} &= 0, \\ v_{\mathrm{w}} &= -\omega a \cos k(x - ct), \\ w_{\mathrm{w}} &= 0, \end{aligned} \right\} \tag{2.2}$$
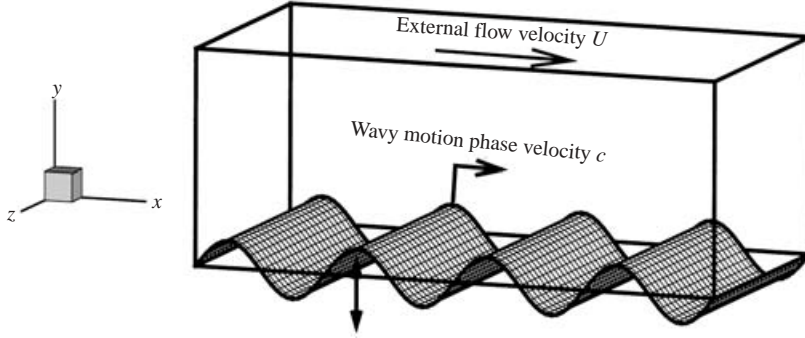
Boundary undergoing up–down motion in the form of a travelling wave

FIGURE 1. Sketch of the physical problem.

where $\omega = kc$ is the frequency of the waving motion, and u, v and w (also denoted as u_1, u_2 and u_3) the velocity components in the x-, y- and z-directions, respectively. Note that if viewed in a frame moving with the phase velocity, the wavy surface becomes stationary and fluid particles on the wall have a non-zero horizontal velocity $-c$. This coordinate transformation facilitates some analysis of the results, which will be discussed in §3.1.

The motions of the flow are described by the Navier–Stokes equations

$$\frac{\partial u_i}{\partial t} = -\frac{\partial p}{\partial x_i} - \frac{\partial (u_i u_j)}{\partial x_j} + \frac{1}{Re}\nabla^2 u_i \qquad (2.3)$$

together with the continuity equation

$$\frac{\partial u_i}{\partial x_i} = 0. \qquad (2.4)$$

Here and hereafter, all variables are normalized by the wavelength λ and the mean velocity of the external flow U unless otherwise indicated. The Reynolds number is defined as $Re \equiv U\lambda/\nu$ with ν the kinematic viscosity. The pressure p is normalized by ρU^2 where ρ is the fluid density.

We apply a free-slip boundary condition at the upper boundary and a periodic boundary condition in horizontal directions.

2.2. Numerical scheme

The Navier–Stokes equation (2.3) subject to the continuity equation (2.4) are advanced in time using a fractional-step method:

$$\frac{\widehat{u}_i - u_i^n}{\Delta t} = \frac{3}{2}\frac{\partial (u_i u_j)^n}{\partial x_j} - \frac{1}{2}\frac{\partial (u_i u_j)^{n-1}}{\partial x_j} + \frac{1}{2}\frac{1}{Re}\nabla^2 u_i^n + \frac{1}{2}\frac{1}{Re}\nabla^2 \widehat{u}_i, \qquad (2.5)$$

$$\frac{u_i^{n+1} - \widehat{u}_i}{\Delta t} = -\frac{\partial \phi^{n+1}}{\partial x_i}. \qquad (2.6)$$

Here the superscript represents the time step and the hat represents the intermediate step. In (2.5), an Adams–Bashforth scheme is used for the convective terms and a Crank–Nicolson scheme is used for the viscous terms. The intermediate velocity solved from (2.5) does not satisfy the continuity equation and ϕ is used in (2.6) as a pressure correction to enforce the velocity at the next step u_i^{n+1} to be divergence-free.

Thus ϕ is governed by a Poisson equation:

$$\nabla^2 \phi = \frac{1}{\Delta t} \frac{\partial \widehat{u}_i}{\partial x_i}. \tag{2.7}$$

For spatial discretization, we use a pseudospectral method with Fourier series in the horizontal directions. In the vertical direction, we use a second-order finite-difference scheme on a staggered grid (Harlow & Welch 1965). A major issue of the simulation of flows near a wavy boundary is that the physical domain is non-rectangular. We use an algebraic mapping to transform the physical space (x, y, z, t) to the computational space (ξ, ψ, ζ, τ) with the following relations:

$$\left. \begin{aligned} \tau &= t, \\ \xi &= x, \\ \psi &= \frac{y - y_{\mathrm{w}}}{H - y_{\mathrm{w}}}, \\ \zeta &= z. \end{aligned} \right\} \tag{2.8}$$

In the above mapping, y_{w} is the location of the moving wall and H the height of the upper boundary. Thus in the computational domain, $\psi = 0$ corresponds to the wavy wall and $\psi = 1$ to the upper boundary.

The algebraic mapping is found to be efficient in our simulations of cases with $ka \lesssim 0.5$. It has been applied to problems with more complicated boundaries such as the interaction of turbulence with free-surface gravity waves and its performance is satisfactory.

It should be noted that in the transformation (2.8), y_{w} is a function of x and t. By applying the chain rule of partial differentiation, we express the Cartesian derivatives as

$$\left. \begin{aligned} \frac{\partial}{\partial t} &= \frac{\partial}{\partial \tau} - v_{\mathrm{w}} \frac{1 - \psi}{H - y_{\mathrm{w}}} \frac{\partial}{\partial \psi}, \\ \frac{\partial}{\partial x} &= \frac{\partial}{\partial \xi} - \frac{\partial y_{\mathrm{w}}}{\partial x} \frac{1 - \psi}{H - y_{\mathrm{w}}} \frac{\partial}{\partial \psi}, \\ \frac{\partial}{\partial y} &= \frac{1}{H - y_{\mathrm{w}}} \frac{\partial}{\partial \psi}, \\ \frac{\partial}{\partial z} &= \frac{\partial}{\partial \zeta}. \end{aligned} \right\} \tag{2.9}$$

The Laplacian becomes

$$\begin{aligned} \nabla^2 = {}& \frac{\partial^2}{\partial \xi^2} + \frac{\partial^2}{\partial \zeta^2} + \frac{1}{(H - y_{\mathrm{w}})^2} \frac{\partial^2}{\partial \psi^2} - 2 \frac{\partial y_{\mathrm{w}}}{\partial x} \frac{1 - \psi}{H - y_{\mathrm{w}}} \frac{\partial^2}{\partial \xi \partial \psi} \\ & + \left[2 \left(\frac{\partial y_{\mathrm{w}}}{\partial x} \right)^2 \frac{1 - \psi}{(H - y_{\mathrm{w}})^2} + \frac{\partial^2 y_{\mathrm{w}}}{\partial x^2} \frac{1 - \psi}{H - y_{\mathrm{w}}} \right] \frac{\partial}{\partial \psi} \\ & + \left(\frac{\partial y_{\mathrm{w}}}{\partial x} \right)^2 \left(\frac{1 - \psi}{H - y_{\mathrm{w}}} \right)^2 \frac{\partial^2}{\partial \psi^2} \end{aligned} \tag{2.10}$$

While it is straightforward to substitute the above operators into equations (2.5)–(2.7), the solving of the Poisson equations needs special care. For rectangular domains with the spectral method in the horizontal directions, each Fourier mode is decoupled from the others and they can be resolved in the vertical direction through a system

of equations. For the present wavy boundary, the grid mapping introduces several nonlinear terms in the Laplacian operator, as shown in (2.10) starting from the third term on the right-hand side. As a result, each Fourier mode is coupled with other modes. To overcome this difficulty, we use an iteration method. Taking equation (2.7) as an example, it is rewritten as

$$
\frac{\partial^2 \phi^{m+1}}{\partial \xi^2} + \frac{\partial^2 \phi^{m+1}}{\partial \zeta^2} + \frac{1}{H^2} \frac{\partial^2 \phi^{m+1}}{\partial \psi^2}
$$
$$
= \frac{1}{\Delta t} \frac{\partial \widehat{u}_i}{\partial x_i} + \left(\frac{1}{H^2} - \frac{1}{(H - y_{\mathrm{w}})^2} \right) \frac{\partial^2 \phi^m}{\partial \psi^2} + 2 \frac{\partial y_{\mathrm{w}}}{\partial x} \frac{1 - \psi}{H - y_{\mathrm{w}}} \frac{\partial^2 \phi^m}{\partial \xi \partial \psi}
$$
$$
- \left[2 \left(\frac{\partial y_{\mathrm{w}}}{\partial x} \right)^2 \frac{1 - \psi}{(H - y_{\mathrm{w}})^2} + \frac{\partial^2 y_{\mathrm{w}}}{\partial x^2} \frac{1 - \psi}{H - y_{\mathrm{w}}} \right] \frac{\partial \phi^m}{\partial \psi} - \left(\frac{\partial y_{\mathrm{w}}}{\partial x} \right)^2 \left(\frac{1 - \psi}{H - y_{\mathrm{w}}} \right)^2 \frac{\partial^2 \phi^m}{\partial \psi^2}.
$$
$$
(2.11)
$$

Here the subscripts m and $m + 1$ represent the previous and current values of the iteration, respectively. A modified Newton's method is used to expedite the convergence of iteration. For the problem considered in this paper, the residual error in ϕ is reduced to $O(10^{-8})$ after less than 10 iterations.

2.3. *Simulation parameters*

We start simulations with DNS results of an open-channel turbulent flow with a flat bottom. The bottom starts to move according to the following formulation:

$$
y_{\mathrm{w}} = a \sin k(x - ct) F(t). \tag{2.12}
$$

Here the factor $F(t)$ is used to make the transition from a flat wall to a travelling wavy wall (equation (2.1)) smooth. It should equal 0 at $t = 0$ and approach 1 as t becomes large. In this study we choose $F(t) = \left[1 - \exp(-t^2) \right]$. Our experience shows that the characteristics of the waving wall boundary layer are fully developed after 10 'flow-through' units of λ/U, i.e. the time required for the external flow to pass a distance of the wavelength λ. After that, we continue the simulation for an additional 30 λ/U to obtain converged statistical results.

The computational domain size is 4λ (streamwise) $\times$ $2/\pi\lambda$ (vertical) $\times$ 2λ (spanwise). It should be noted that the use of periodic boundary conditions in the horizontal directions implies that flow exiting one face of the boundary enters the opposite one. It is thus important to ensure that the domain size is sufficiently larger than the largest eddy in question. To confirm this, we consider the two-point correlation coefficient in the streamwise direction:

$$
R_{u_i u_i}(\xi; \psi) = \frac{\displaystyle\iint u_i'(\xi', \psi, \zeta') u_i'(\xi' + \xi, \psi, \zeta') \, \mathrm{d}\xi' \, \mathrm{d}\zeta'}{\displaystyle\iint u_i'^2(\xi', \psi, \zeta') \, \mathrm{d}\xi' \, \mathrm{d}\zeta'}, \qquad \text{no summation for } i. \tag{2.13}
$$

Here u' is the velocity fluctuation defined as the instantaneous value subtracted by the value averaged over the spanwise direction. Figure 2 plots values of $R_{u_i u_i}$. For comparison, we also plot the results when half of the domain size (two wavelengths in the streamwise direction) is used for simulation. It is shown that except for the streamwise velocity component, the correlation is close to zero over a separation distance of λ; while for a distance of 2λ, all the correlation coefficients vanish. In this study we choose 4 wavelengths as the streamwise domain size. We remark that this
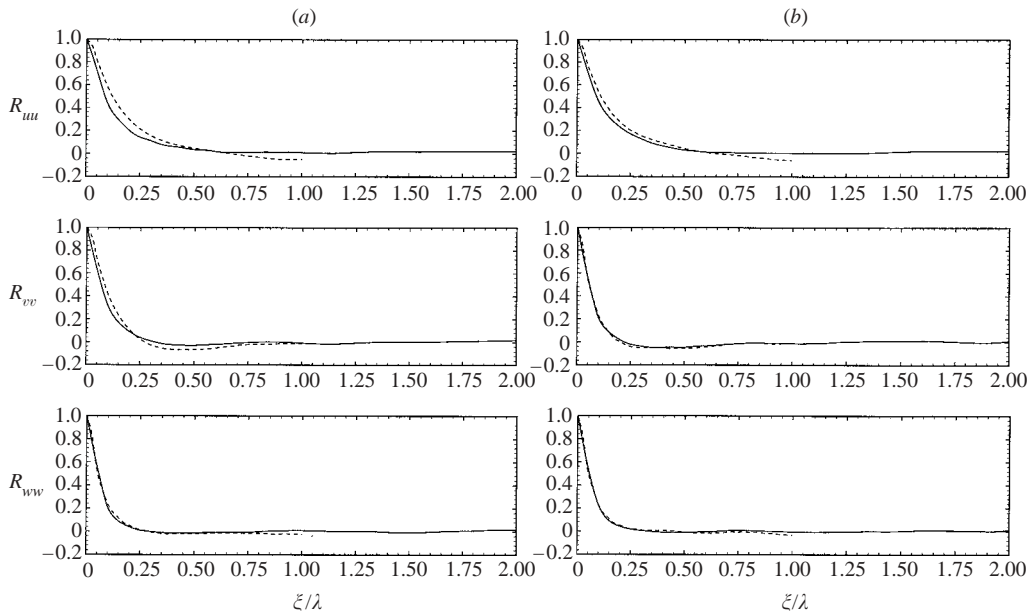
FIGURE 2. Streamwise two-point correlation function $R_{u_i u_i}(\xi)$ at (a) $\psi = 0.05$, and (b) $\psi = 0.2$. ————, Streamwise domain size 4λ; $----$, streamwise domain size 2λ.

choice is consistent with other numerical studies on fixed wavy walls (e.g. Cherukat *et al.* 1998 used 4 wavelengths, De Angelis *et al.* 1997 used 3 and 6, and Calhoun & Street 2001 used 2).

An evenly spaced grid with 192 points is used in both the streamwise and spanwise directions. In the vertical direction, we use a 192-point grid which is clustered towards the wall. The first grid is about 0.2 wall units away from the wall. In the external flow, the spacing of the vertical grid is about 2 wall units. We remark that compared to simulations of turbulent channel flows, the vertical grid in the bulk flow is more dense in the present study. The reason is that for certain phase speed (e.g. when $c = 0$), flow separation occurs after the flow passes the crest and there exists a free shear layer. The shear layer plays an important role in the production of turbulence (cf. Hudson *et al.* 1996) and it is essential to resolve this layer. In the future, it would be desirable to have an adaptive grid which distributes the grid points according to the physics of the simulation results so that the computational cost can be reduced.

To ensure that the current 192^3 grid is sufficient in resolving all the dynamically significant scales of the flow, we also perform a low-resolution simulation with a 96^3 grid. For all the results presented in this paper the two sets of simulations have been compared and the difference is found to be negligible. A typical example is shown in figure 3 which plots the distribution of pressure and x-component of friction force on the wall. The difference between the two simulations with different resolutions is small and it can be concluded that a grid-independent solution has been obtained.

The results in figure 3 are first averaged in the spanwise direction and then averaged with respect to the phase of the wavy wall according to the following relation:

$$x - ct = x' + n\lambda, \tag{2.14}$$

where n is an integer and $0 \leqslant x' < \lambda$. As plotted in figure 3(b), the crest is located at $x'/\lambda = 0.25$ and the trough is at $x'/\lambda = 0.75$. Hereafter, for any variable $f(x, y, z, t)$,
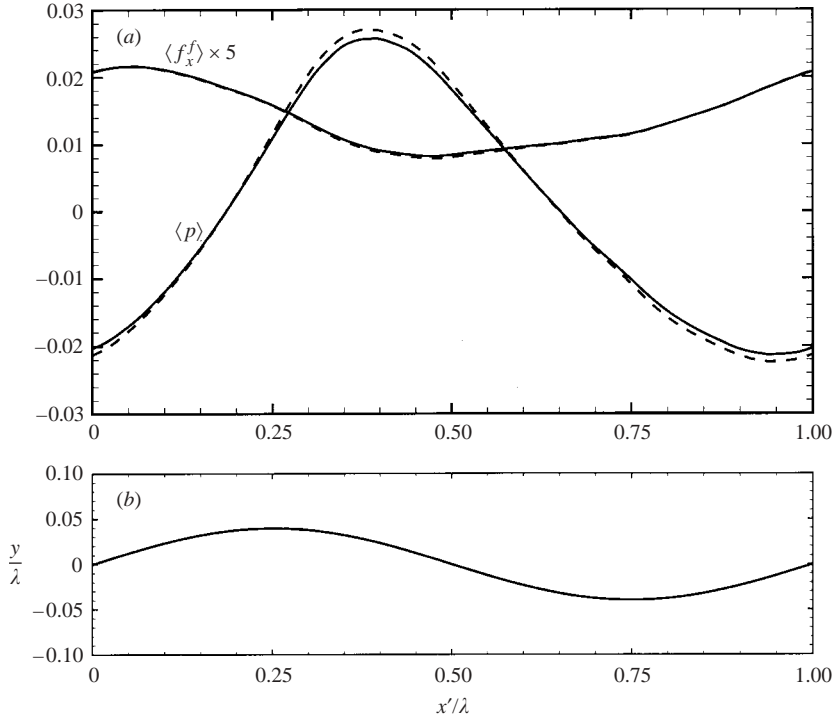
FIGURE 3. (*a*) Distribution of the mean pressure $\langle p \rangle$ and x-component of friction force $\langle f_x^f \rangle$ along the wavy surface for: – – – –, high-resolution simulation using 192^3 grid points; and ———, low-resolution simulation using 96^3 grid points. $c/U = 0.4$. The results are obtained using phase averaging relative to that of the (moving) wavy surface $y_w = a \sin(kx')$ shown in (*b*).

its averaged value $\langle f \rangle(x', z)$ is defined as first averaged in the spanwise direction and then phase-averaged according to (2.14). We use $f'(x, y, z, t) \equiv f(x, y, z, t) - \langle f \rangle(x', z)$ to denote the fluctuation.

In the present paper we focus on the case with $Re \equiv U\lambda/\nu \approx 10,170$ and $ka = 0.25$. A variety of phase speeds ranging from $c/U = -1$ to 2 at intervals of 0.2 are considered. For each phase speed, extensive DNS is performed on a 192^3 grid with 40 flow-through time units U/λ to obtain converged statistics. The simulation cost of this study is substantial and through it we obtain an overall picture of the effects of the phase speed of the wall waving motion on the turbulent boundary layer, the drag force, and the power consumption.

3. Results

In this section we present the results, with a focus on the effects of the phase velocity of the wall waving motion. In §3.1 we use the streamline topology of the mean flow field and mean velocity contours to provide an overall picture of the turbulent boundary layer near a travelling wavy wall. The turbulence statistics are then illustrated in §3.2 with the focus on the laminarization effects of the wall waving motion. Finally in §3.3 we analyse the drag force acting on the wavy wall and power consumption, which is essential to the study of the fish swimming mechanism. We will show that as the phase speed of the travelling wave wall motion increases, the

drag force decreases and turns into a thrust. The power consumption, on the other hand, decreases first, reaching a minimum at $c/U \approx 1.2$, and then increases.

3.1. *Mean flow*

Figure 4 plots the streamline pattern of the mean flow $(\langle u \rangle, \langle v \rangle)$, contours of $\langle u \rangle$ and $\langle v \rangle$, and contours of the magnitude of the mean velocity $(\langle u \rangle^2 + \langle v \rangle^2)^{1/2}$. Representative cases with different travelling velocity of the wavy wall $c/U = 0, 0.4, 1.2, 2$, and -0.4 are shown.

When the wall is stationary ($c/U = 0$), the flow might separate after it passes the crest if the wave is sufficiently steep. For the present simulations with a wavy wall steepness $ka = 0.25$, the streamlines in figure 4(*a*) show a separation bubble located on the downhill side of the wavy wall. The appearance of the separation bubble for the current simulation parameters is consistent with the prediction by Kuzan *et al.* (1989) (cf. the flow regime map provided in their figure 1). Over the lower half of the separation bubble, the streamwise velocity $\langle u \rangle$ is negative (flow reverses) and the vertical velocity $\langle v \rangle$ is positive. It is shown that the reversed flow exists between $x'/\lambda \approx 0.42$ and $x'/\lambda \approx 0.81$. It should be noted that the flow separation is highly intermittent (Hudson *et al.* 1996) and figure 4 only represents an averaged effect. From the streamline pattern and contours of velocity magnitude $(\langle u \rangle^2 + \langle v \rangle^2)^{1/2}$ plotted in figure 4(*a*), it is clear that the flow can be divided into four regimes (Buckles *et al.* 1984): an outer flow, a separated region, an attached boundary on the uphill side of the wavy wall, and a free shear layer which is located behind the crest and is characterized by a large velocity gradient.

When wavy wall displacement travels in the streamwise direction, substantially new physics are added to the picture. In addition to the turbulent boundary layer with an outer flow velocity U, there are also secondary motions caused by the up–down oscillation of the wall. The latter has a velocity of $O(kac)$ and its significance increases with the phase velocity of the waving motion c. Since the wall is in motion, the wall boundary is no longer a streamline and there are streamlines that emanate from (and end on) the surface.

We first examine in figure 4(*b–d*) the effect of positive c/U. As the wave travels from left to right, the right side of the crest rises and the left side descends. The contours of $\langle v \rangle$ shows that as c/U increases from 0.4 to 1.2 to 2.0, the vertical flow induced by the wall waving motion increases significantly. As a result, while the streamlines above the trough are concave at $c/U = 0$, they become flat at $c/U = 0.4$ and even convex at $c/U = 1.2$ and $c/U = 2.0$.

Comparison of the contours of $\langle u \rangle$ and $(\langle u \rangle^2 + \langle v \rangle^2)^{1/2}$ in figure 4(*b–d*) with those in figure 4(*a*) shows that the wall travelling wave motion tends to suppress flow separation. The free shear layer shown at $c/U = 0$, which is formed by the detachment of the boundary layer from the surface and characterized by a large shear rate and diverged velocity magnitude contours, becomes less obvious at $c/U = 0.4$. No flow reversal region ($\langle u \rangle < 0$) is found at $c/U = 0.4$. At $c/U = 1.2$ the flow becomes smoother and contour lines of the velocity magnitude are parallel to the wave surface. As the phase velocity becomes even larger, $c/U = 2$, the wavy wall forward of the crest pushes the fluid at so strongly that there is a flow reversal region above the crest. One implication of this is that the friction force and the turbulence production mechanism are affected by c/U. This is indeed true and will be shown in later sections.

Figure 4(*e*) shows the effects of negative c/U, i.e. wave travelling against the external flow. Compared to figure 4(*a*), the negative $c/U = -0.4$ results in larger area of flow
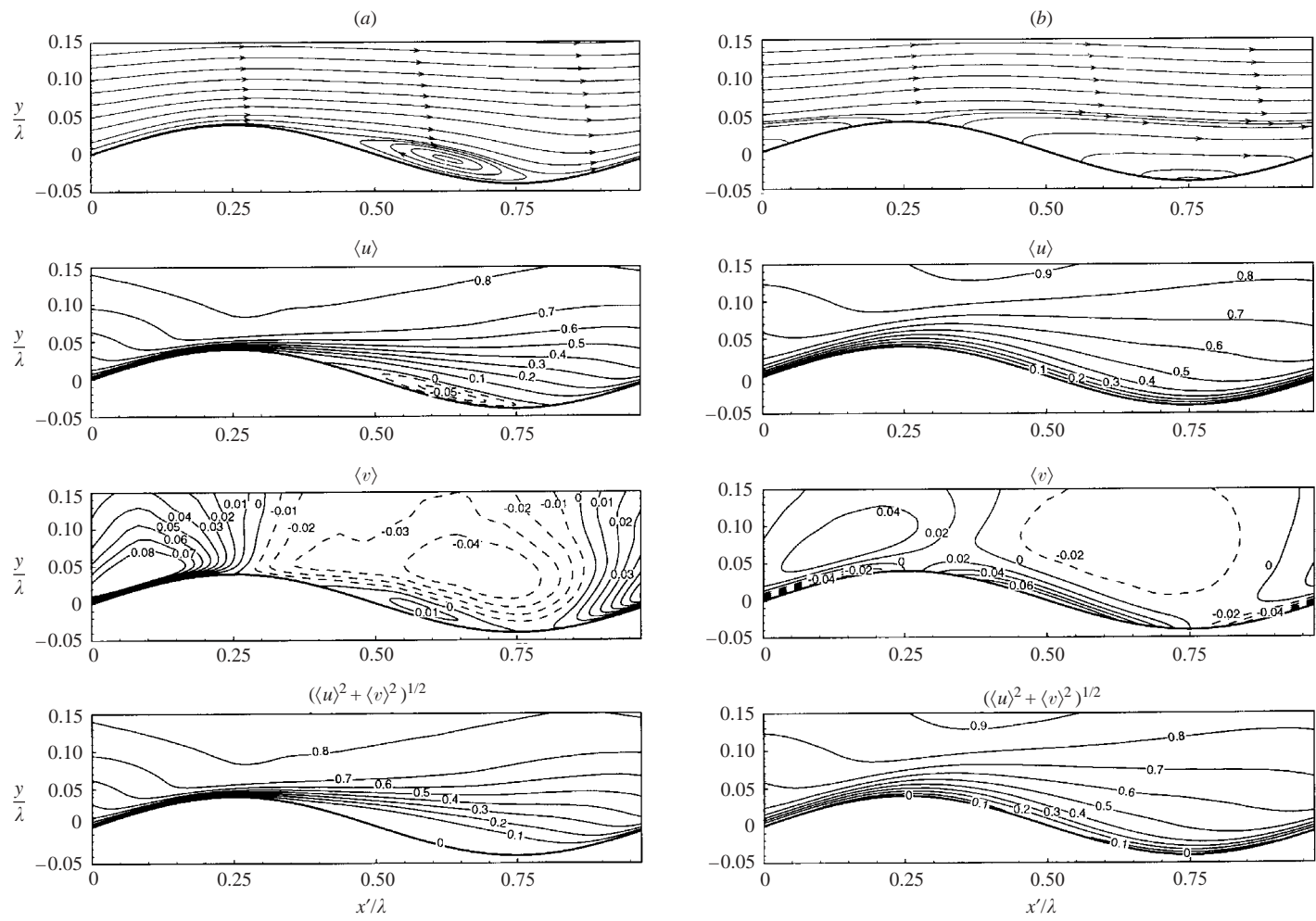
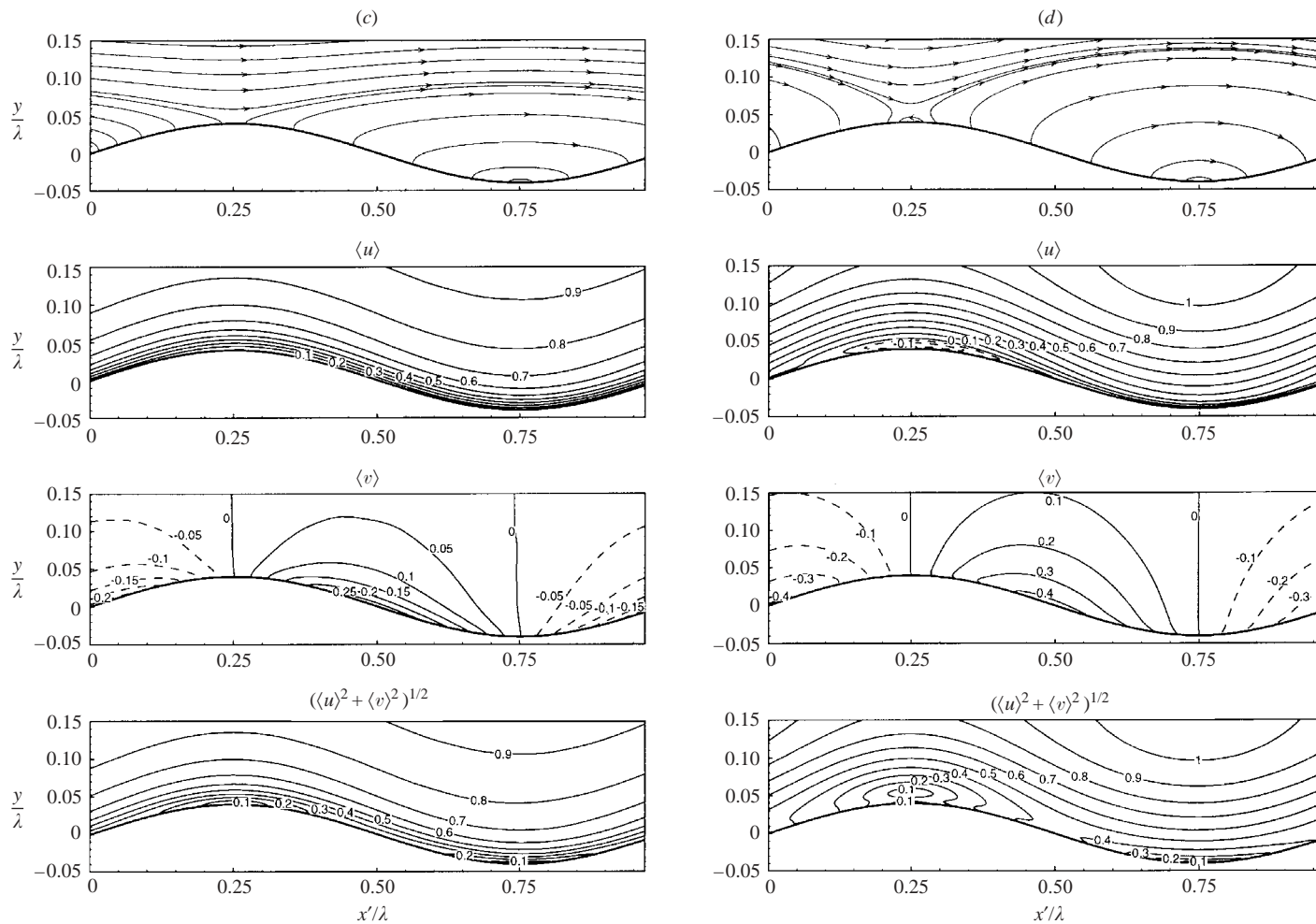FIGURE 4(a, b). For caption see page 208.
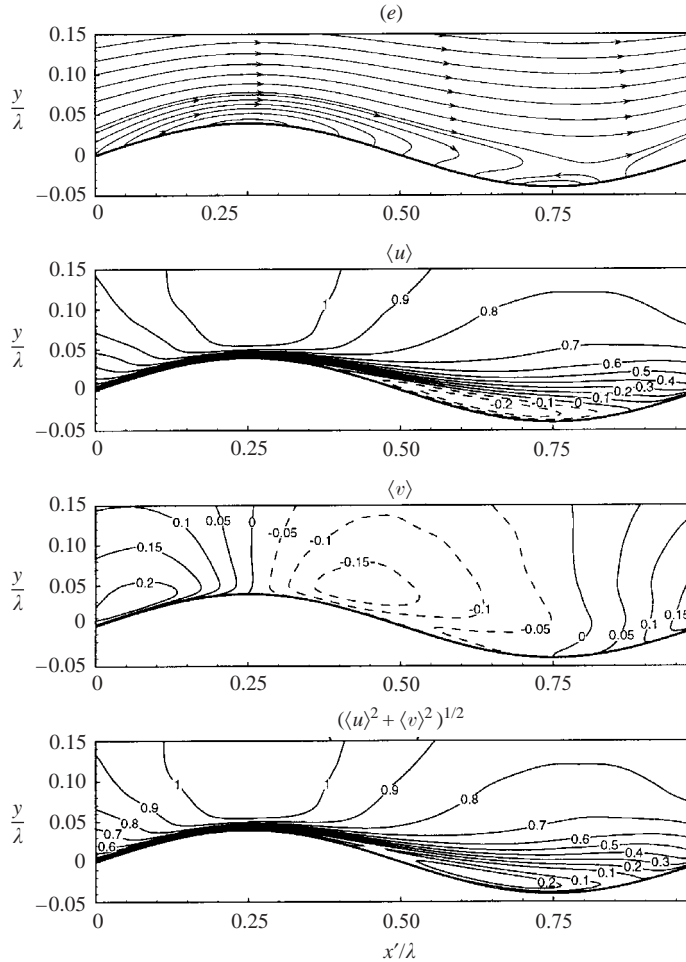
FIGURE 4(c, d). For caption see page 208.

FIGURE 4. Streamline pattern of the mean flow (top) and spatial variation of $\langle u \rangle$, $\langle v \rangle$ and $(\langle u \rangle^2 + \langle v \rangle^2)^{1/2}$ for phase velocities of: (*a*) $c/U = 0$; (*b*) $c/U = 0.4$; (*c*) $c/U = 1.2$; (*d*) $c/U = 2$; and (*e*) $c/U = -0.4$. Dashed contour lines represent negative values.

reversals, larger magnitude of negative $\langle u \rangle$, and a stronger free shear layer. It is clear that negative c/U has the opposite effects to positive c/U.

As pointed out earlier, some streamlines emanate from and end at the wave surface if the wavy wall travels. As a result, the boundary is no longer a streamline and flow patterns such as recirculation cannot be identified based on streamline topology. This difficulty can be overcome if the frame is moving with the wave. In the new frame, the mean velocity is given by $(\langle u \rangle - c, \langle v \rangle)$. The wavy profile become stationary in time (but with non-zero tangential velocity). We remark that this approach also simplifies the numerical scheme by eliminating the time-derivative terms in grid mapping, at the expense of modifying the velocity boundary conditions according to the phase velocity of the wave.

In the moving frame, the velocity at the wall is

$$\left.\begin{array}{l} \widetilde{u}_w = -c, \\ \widetilde{v}_w = -cka\cos{(kx)}. \end{array}\right\} \tag{3.1}$$
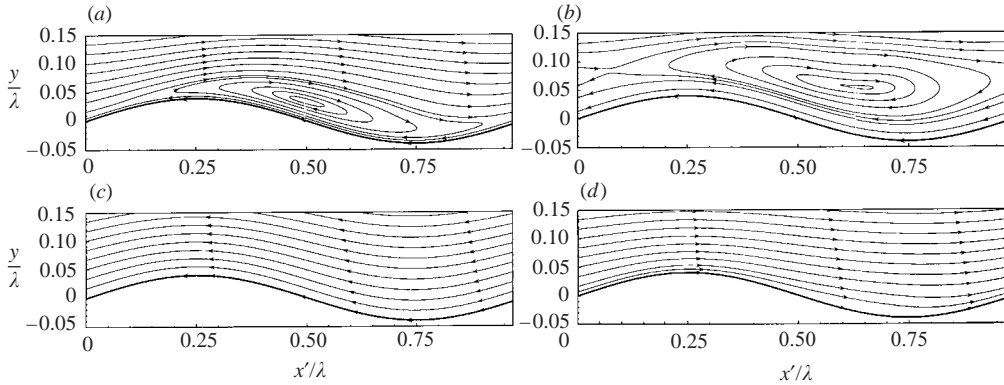
FIGURE 5. Streamline pattern of the mean flow in a frame moving with the phase velocity c for: (a) $c/U = 0.4$; (b) $c/U = 0.8$; (c) $c/U = 1.2$; and (d) $c/U = -0.4$. Note that for $c/U = 0$, the result is the same as in figure 4(a).
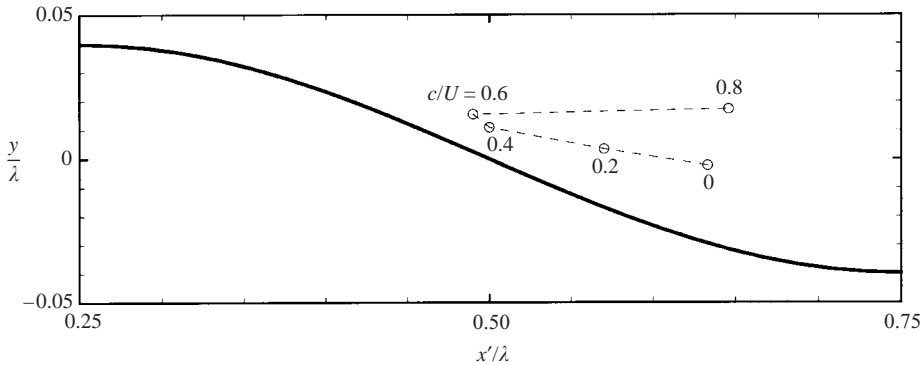

FIGURE 6. Centre of the trapped vortex for different phase speeds of the wavy wall.

As a result, the magnitude of velocity on the wall is $c[1 + (ka)^2 \cos^2(kx)]^{1/2} \geqslant c$, which reaches its maximum value of $c[1 + (ka)^2]^{1/2}$ at wave nodal points and retains its minimum value of c at crests and troughs. We also obtain from (3.1) that

$$\frac{\widetilde{v}_w}{\widetilde{u}_w} = ka \cos(kx) = \frac{\mathrm{d}y_w}{\mathrm{d}x}, \tag{3.2}$$

which means that fluid particles are gliding along the wall, as shown in figure 5.

In the moving frame, the horizontal velocity component equals $-c$ at the wall and $U - c$ far away. Therefore, if $0 < c < U$, the mean velocity must change its sign as the wall is approached from the outer region. The streamlines plotted in figures 5(a) and 5(b) show a trapped vortex located near the negative wave slope region for both $c/U = 0.4$ and 0.8. Note that for $c/U = 0$ the result is identical to figure 4(a). This phenomenon resembles the 'critical layer' described by Miles (1957) and the 'cat's-eyes' sketched by Lighthill (1962). As c/U increases, the extent of the vortex increases. Figure 6 plots the location of the vortex core as a function of c/U. As expected, the vortex centre (where $\widetilde{u} = \widetilde{v} = 0$) moves away from the wall as c/U increases, because of the increase in the magnitude of the vertical and horizontal velocities (both proportional to c) at the wall (and the decrease in the effective free-stream velocity $U - c$). The horizontal movement of the vortex core can be qualitatively
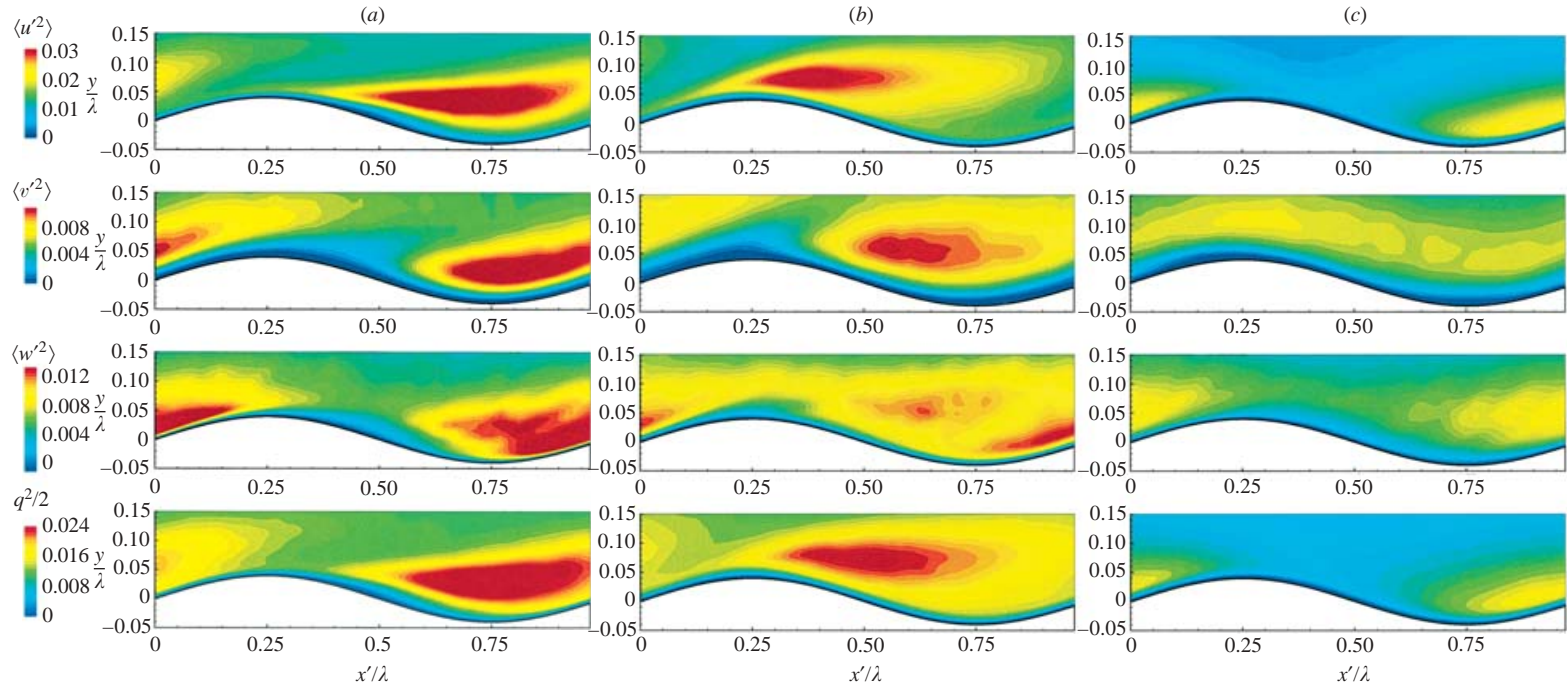
FIGURE 7. Contours for $\langle u'^2 \rangle$, $\langle v'^2 \rangle$, $\langle w'^2 \rangle$ and turbulence kinetic energy $q^2/2 \equiv \langle (u'^2 + v'^2 + w'^2)/2 \rangle$ for: (a) $c/U = 0$; (b) $c/U = 0.4$; and (c) $c/U = 1.2$. Note that the contour scales are identical for all the c/U cases (but different for different velocity components).
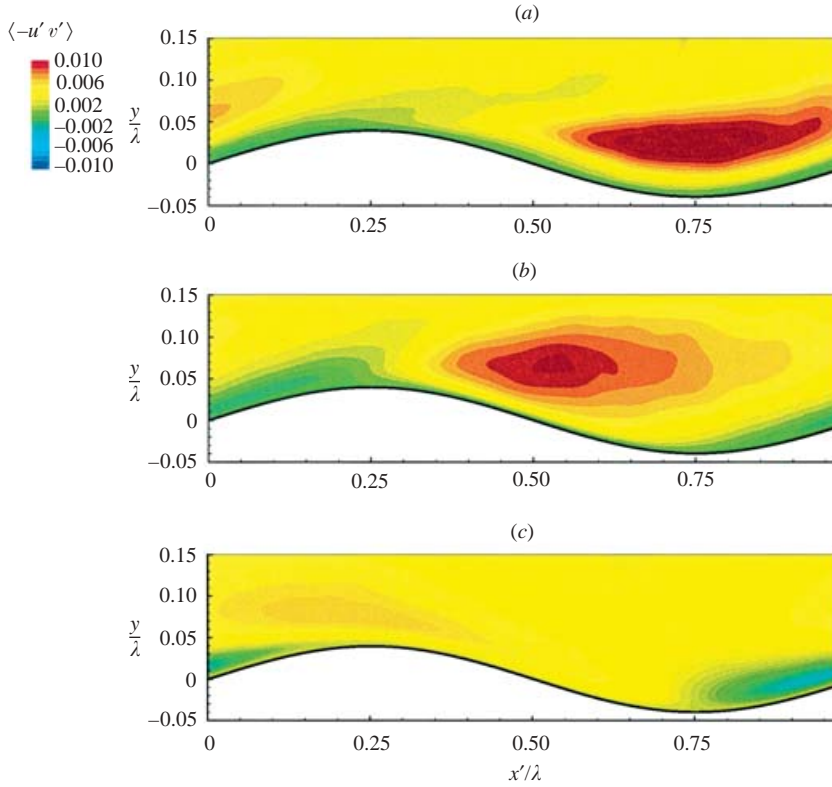
FIGURE 8. Contours of Reynolds stress $\langle -u'v' \rangle$ for: (a) $c/U = 0$; (b) $c/U = 0.4$; and (c) $c/U = 1.2$.

understood: for relative small c/U (> 0), the separation eddy moves upstream with increasing c/U due to the increasing (negative) wall tangential/horizontal velocity (in the moving frame). As c/U further increases, the eddy is displaced vertically from the wall and is influenced more by the free stream than the wall (velocity) and hence is washed further downstream.

If the phase velocity of the wave exceeds the external flow velocity, both $-c$ and $U - c$ are negative. Figure 5(c) shows that at $c/U = 1.2$, all the streamlines are in the negative x-direction and there is no trapped vortex. Nor does the vortex exist for $c/U = -0.4$ (figure 5d) as both the wall ($-c$) and the external flow ($U - c$) are moving in the positive x-direction in the moving frame.

3.2. *Turbulence fluctuations*

Wavy wall motion strongly modifies not only the mean flow but also the turbulence intensities. Figure 7 compares the turbulence intensities of each velocity component $\langle u_i'^2 \rangle$ and turbulent kinetic energy $q^2/2 \equiv \langle (u'^2 + v'^2 + w'^2)/2 \rangle$ for $c/U = 0$, 0.4 and 1.2.

When the wavy wall is stationary ($c/U = 0$), figure 7(a) shows that the maximum streamwise velocity fluctuation exists above the trough and behind the crest, the location of which corresponds roughly to the free shear layer. The maximum of the vertical velocity intensities lags the streamwise one. The spanwise velocity component, on the other hand, has its maximum fluctuation located near the uphill region where reattachment takes place. Among the three velocity components, the streamwise one

contributes most to the turbulent kinetic energy. These results agree well with existing measurements (e.g. Hudson *et al.* 1996) and simulations (e.g. De Angelis *et al.* 1997; Cherukat *et al.* 1998; and Calhoun & Street 2001) of flows past a fixed wavy wall.

When the wavy wall has a downstream phase velocity $c/U = 0.4$, it is shown in figure 7(*b*) that the locations of the maxima of streamwise and vertical fluctuations move upstream compared to the $c/U = 0$ case. This relocation is consistent with the upstream movement of the trapped vortex shown in §3.1. The spanwise velocity appears to have two maxima, one located near the reattachment position and the other above the trough. The reason for the former can be attributed to the pressure–strain correlation as the fluid impacts on the backward face of the wavy wall, while the latter is related to energy transferred to the spanwise direction from streamwise and vertical velocity fluctuations produced by the free shear layer. Compared to the $c/U = 0$ case, turbulence intensity is reduced at $c/U = 0.4$ because of the weakening in the flow separation.

It is interesting to note that as the phase speed of the wall motion increases to $c/U = 1.2$, the turbulence intensity is substantially reduced in most of the region, e.g. above the forward facing surface (where the highest turbulence energy is located for low c/U). This laminarization effect can be attributed to the elimination of flow separation, which is the major mechanism for turbulence production for flows past a stationary wavy wall (cf. Hudson *et al.* 1996).

The Reynolds stress $\langle -u'v' \rangle$ plotted in figure 8 is consistent with the findings for the turbulence intensities. For $c/U = 0$, the greatest Reynolds stress occurs near the location of the free shear layer. When the wavy wall has a small phase velocity $c/U = 0.4$, $\langle -u'v' \rangle$ is reduced and its maximum moves upstream. At $c/U = 1.2$, $\langle -u'v' \rangle$ becomes very small and its maximum is located upstream of the wave crest in contrast to the small c/U cases.

The laminarization effects at $c/U = 1.2$ can also be seen from the streamwise velocity profiles plotted in figure 9, where both the velocity and vertical distance are normalized by the wall units:

$$u^+ = \frac{u}{(\tau/\rho)^{1/2}}, \quad y^+ = \frac{y - y_{\mathrm{w}}}{(\rho \nu^2/\tau)^{1/2}}. \tag{3.3}$$

Here τ is the local shear stress. At regions of flow reversal, for example near $x'/\lambda = 0.5$ and 0.75 for $c/U = 0$, τ is negative and the above definition is not applicable.

Figure 9 compares $c/U = 0, 0.4$ and 1.2 at $x'/\lambda = 0, 0.25, 0.5$ and 0.75. For reference, figure 9(*a*) also plots the law of the wall for a flat wall and the DNS results for this case using the same code. The agreement and resolution are satisfactory. For the present problem, because of the surface curvature and velocity, the flat-plate profile should not be expected. Figure 9 shows that the velocity profile is strongly affected by the phase velocity (and phase) of the wall waving motion. Of special interest is the $c/U = 1.2$ case where there is an extended viscous inner layer. This phenomenon is caused by the laminarization effects discussed above: the turbulence fluctuations and Reynolds stress are substantially suppressed at $c/U \approx 1.2$ and, as a result, the laminar viscous effect becomes relatively more important. Note that this laminarization effect is non-uniform relative to the wavy wall phase. This can be compared with the large spatial variations of the turbulence fluctuations in figures 7 and 8 as c/U changes. Finally, we remark that similar behaviours have been observed in recent experimental measurements using laser Doppler velocimetry and digital particle image velocimetry at MIT (cf. Techet 2001).
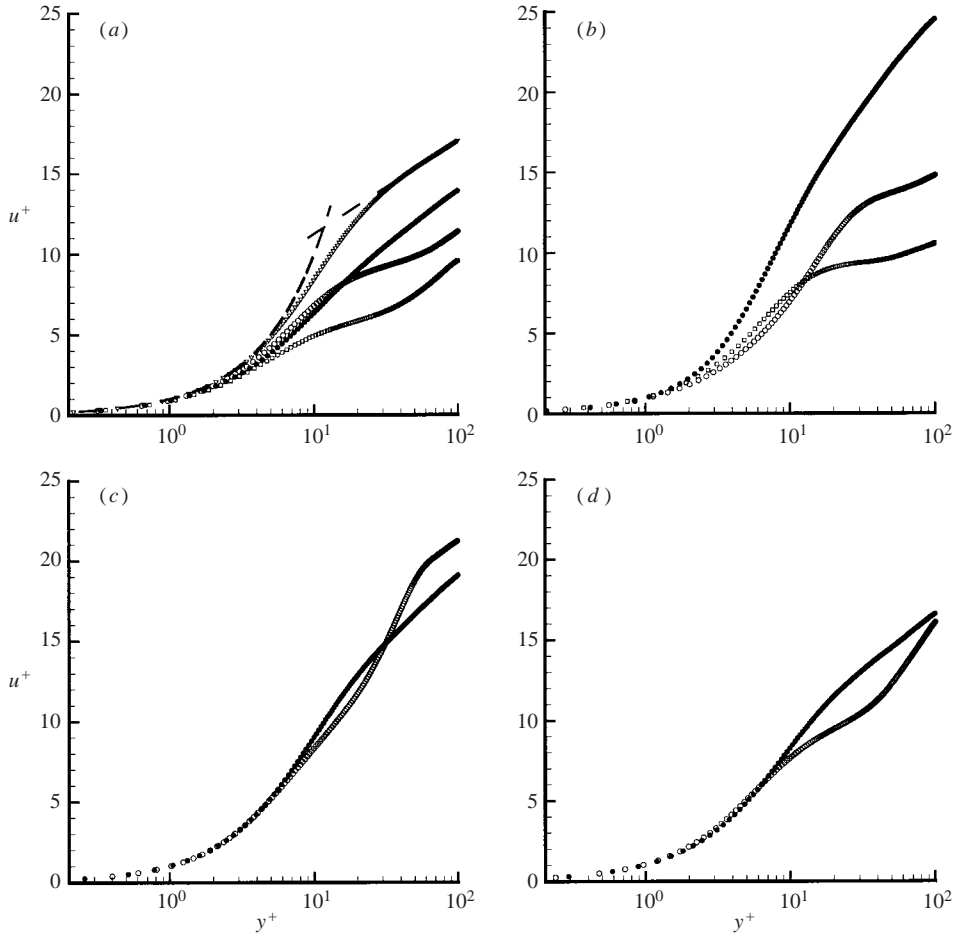
FIGURE 9. Computed data of streamwise velocity at: (*a*) $x'/\lambda = 0$; (*b*) $x'/\lambda = 0.25$; (*c*) $x'/\lambda = 0.5$; and (*d*) $x'/\lambda = 0.75$. $\square$, $c/U = 0$; $\bigcirc$, $c/U = 0.4$; $\bullet$, $c/U = 1.2$. In (*a*), the dashed lines represent the law of the wall for a flat plate and the $\triangledown$ represents the DNS results using the same code.

The pronounced effects of the wall motion on the turbulence fluctuations can also be seen from the instantaneous vortex structure plotted in figure 10 where we contrast the results for $c/U = 0$ and $c/U > 0$. To identify the vortices, we plot the isosurfaces of the second largest eigenvalue of the tensor $\mathbf{S}^2 + \Omega^2$, with $\mathbf{S}$ and Ω respectively the symmetric and antisymmetric parts of the velocity gradient tensor $\nabla\mathbf{v}$ (Jeong & Hussain 1995). For $c/U = 0$, the dominant vortex structures are located above the trough and are generally less coherent than the $c/U > 0$ cases. In particular, it is relatively difficult to distinguish between the streamwise and spanwise structures. The instantaneous vortical structures are substantially modified for positive c/U. Figure 10(*b*) shows a representative case for $c/U = 1.2$ (where the turbulence suppression is maximum in figures 7 and 8). The structures are substantially coherent and dominated by streamwise elements. The vorticity dynamics for this flow is now strongly influenced by the non-zero tangential velocity. The details are of much interest and this is a subject of our on-going investigation.
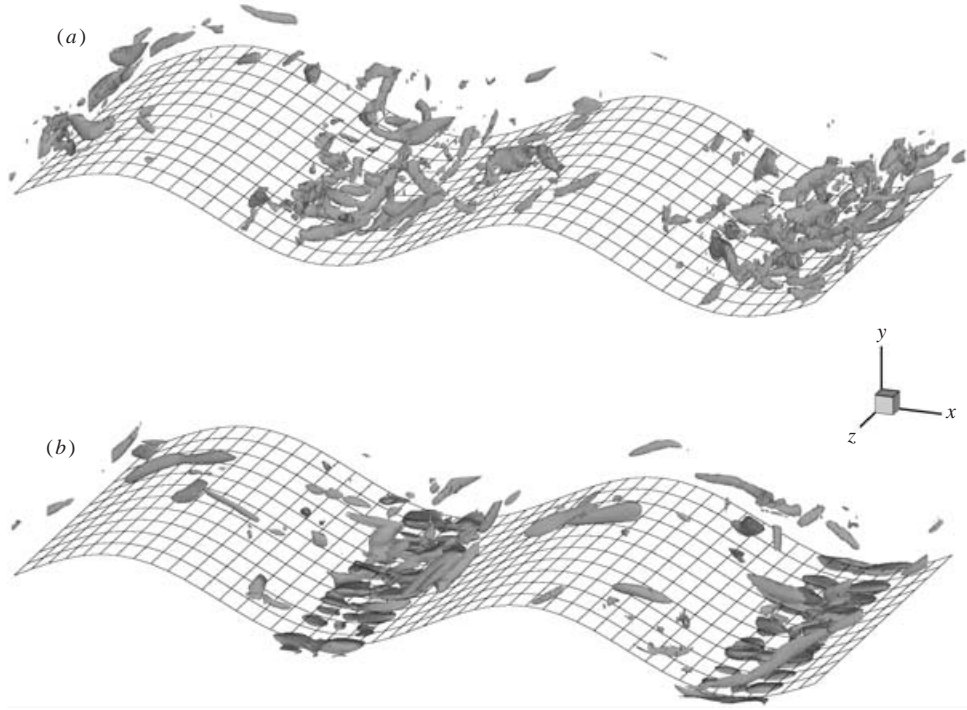
(a)

(b)

y

x

z

FIGURE 10. Vortex structure for (a) $c/U = 0$ and (b) $c/U = 1.2$.

3.3. Drag force and power consumption

In this section we analyse the drag force acting on the wavy surface and the power needed for it to be propelled, which are directly relevant to the study of fish locomotion.

The total drag (longitudinal) force on the wavy surface consists of a friction drag and a form drag. As shown in figure 1, for an element of the wall surface $ds = [1+(dy_w/dx^2)]^{1/2} dx$, its tangential direction is $t = (1, dy_w/dx)[1+(dy_w/dx)^2]^{-1/2}$ and the wall-normal direction is $n = (-dy_w/dx, 1)[1 + (dy_w/dx)^2]^{-1/2}$. The friction force and pressure force per unit area (projected on the (x, z)-plane) are respectively

$$\left. \begin{aligned} f_x^f &= \mu \left[-2\frac{\partial u}{\partial x}\frac{dy_w}{dx} + \left(\frac{\partial u}{\partial y} + \frac{\partial v}{\partial x} \right) \right] \quad \text{on} \ \ y = y_w, \\ f_x^p &= p\frac{dy_w}{dx} \quad \text{on} \ \ y = y_w. \end{aligned} \right\} \tag{3.4}$$

By integrating f_x^f and f_x^p over the wavy surface, we obtain the total friction force F_f, the pressure force F_p, and the total drag force $F_d = F_f + F_p$.

Figure 11 plots the variations of F_f, F_p and F_d as functions of the phase speed of the wall waving motion c/U, while their values at select c/U are listed in table 1. The friction force is always positive and its variation is relatively small. It has a local minimum around $c/U = 0$. As c/U increases from $c/U = 0$ to 2, it first increases and then decreases slightly. The pressure force F_p, on the other hand, decreases monotonically as c/U increases. Near $c/U = 1$, F_p changes sign from positive to negative, i.e. becomes a thrust rather than a drag for $c \gtrsim 1$. The total drag
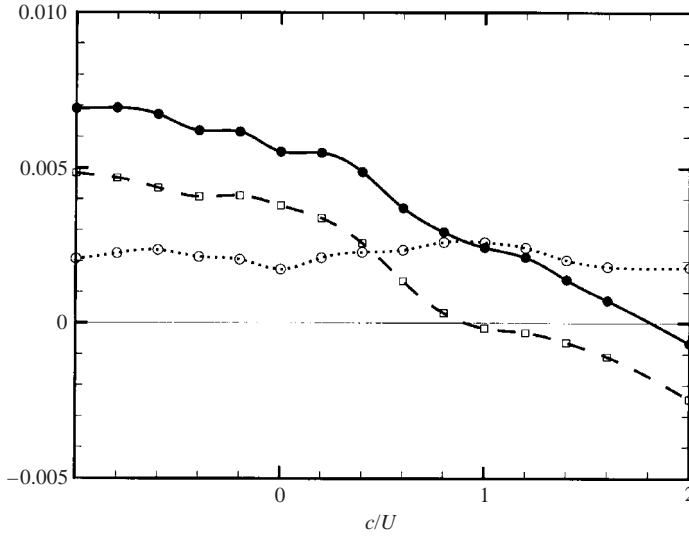
FIGURE 11. Variation of the drag force acting on a wall undergoing travelling wave motion as a function of c/U. $\cdot\,\odot\,\cdots\cdot$, friction drag F_f; $\square$ $--$, form drag F_p; $-\!\!\bullet\!\!-$, total drag $F_d = F_f + F_p$.

c/U	F_f	F_p	$F_d = F_f + F_p$	P_S	P_D	$P_T = P_S + P_D$
−1.0	0.00208	0.00484	0.00691	0.00481	0.00691	0.01172
−0.4	0.00214	0.00407	0.00621	0.00160	0.00621	0.00781
0	0.00174	0.00379	0.00553	0	0.00553	0.00553
0.4	0.00229	0.00253	0.00487	−0.00101	0.00487	0.00387
0.8	0.00261	0.00032	0.00294	−0.00037	0.00294	0.00257
1.2	0.00243	−0.00031	0.00212	0.00011	0.00212	0.00223
1.6	0.00181	−0.00109	0.00072	0.00256	0.00072	0.00329
2.0	0.00179	−0.00245	−0.00066	0.00727	−0.00066	0.00661

TABLE 1. Friction drag force F_f, pressure drag force F_p, total drag force $F_d = F_f + F_p$; and swimming power P_S, drag force power P_D, and total power $P_T = P_S + P_D$ required to propel a wavy wall for select value of the relative phase speed c/U.

F_d ($= F_f + F_p$) decreases as c/U increases. At large c/U (≈ 2), F_d becomes negative (thrust force).

To explain the effects of c/U on the drag force, we first examine the distribution of f_x^f along the wavy surface. Figure 12 compares cases at $c/U = 0$, 0.4, 1.2 and 2.0. The different c/U curves show substantial variations as functions of phase and relative to each other. For $c/U = 0$, the friction force increases rapidly after the reattachment where the boundary layer starts (cf. figure 4*a*) and decreases thereafter. Its value is negative over the trough because of flow reversals. For $c/U = 0.4$ and 1.2, the variation of f_x^f becomes milder. It is positive over the entire domain because, as §3.1 shows, there is no flow reversal. For $c/U = 2$, the friction force becomes negative above the crest as a result of flow reversal there (figure 4*d*). Figure 12 shows that the magnitude of this negative f_x^f is large, which indicates strong shear in the reversed flow near the crest. The reappearance of flow reversals contributes to the decrease of the net friction drag at large c/U shown in figure 11.
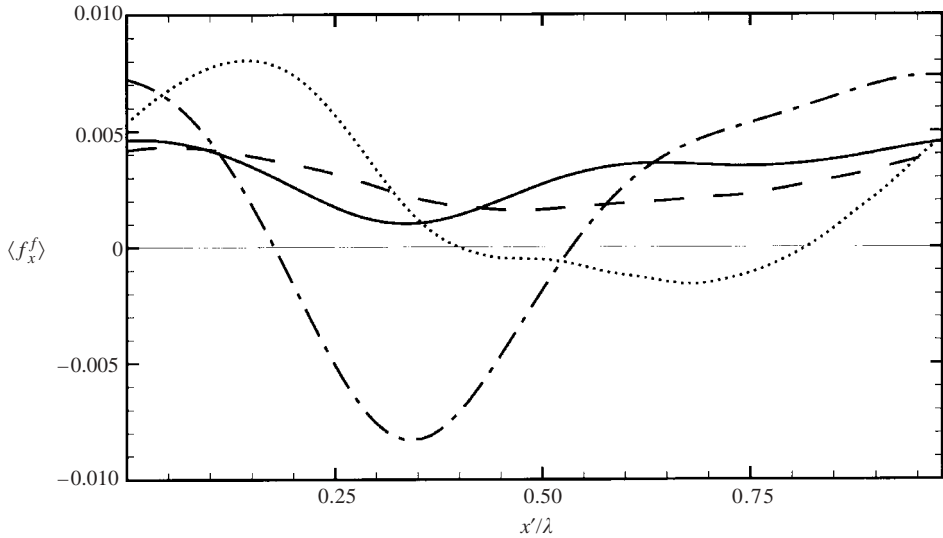
FIGURE 12. Distribution of the x-component of friction force acting on the wavy wall.
$\cdots\cdots$, $c/U = 0$; $----$, $c/U = 0.4$; ———, $c/U = 1.2$; $-\cdot-\cdot-$, $c/U = 2$.
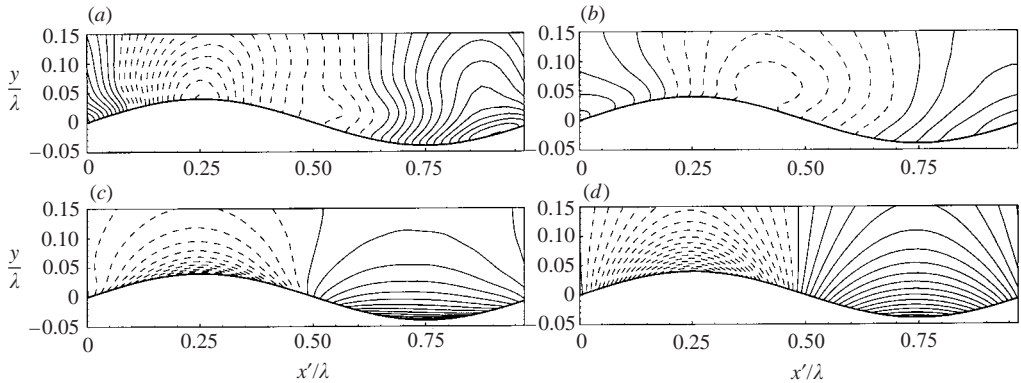

FIGURE 13. Contours of the mean pressure $\langle p \rangle$ for: (a) $c/U = 0$; (b) $c/U = 0.4$; (c) $c/U = 1.2$; and (d) $c/U = 2$. Dashed lines represent negative values. Contour intervals are 0.005 in (a–c) and 0.025 in (d).

We next investigate the form drag due to pressure. The phase-averaged pressure contours are plotted in figure 13, which shows substantial difference between low and high values of c/U. If the wavy wall is stationary ($c/U = 0$), the pressure variation is asymmetric about the crest (and the trough) because of the (asymmetric) position of flow separation and reattachment. This result is consistent with previous studies (e.g. Cherukat *et al.* 1998). For small values of c/U ($= 0.4$ say), the magnitude of the pressure variation is reduced, which can be explained by the weakening of the flow separation. The overall distribution of the pressure is, however, similar to the $c/U = 0$ case. As c/U becomes larger, figures 13(c) and 13(d) show that the pressure distribution becomes more symmetric, and is almost completely so as flow separation is eliminated near $c/U = 1.2$ (cf. §3.1).

More importantly, for larger values of c/U, the pressure is now mainly controlled by wall-normal velocities (in the non-moving frame) rather by flow separation.
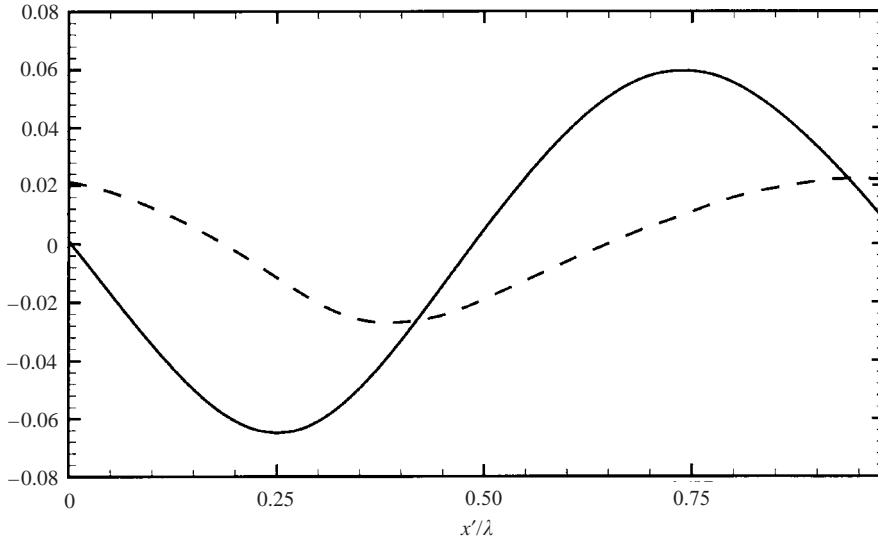
FIGURE 14. Distribution of mean pressure $\langle p \rangle$ on the wavy wall.
$----$, $c/U = 0.4$; ————, $c/U = 1.2$.

Alternatively, viewed in a frame moving with c, the pressure gradients are primarily driven by the tangential flow over the curved surface (figure 5). In either case, the magnitude of the (wall-normal) pressure gradient (proportional to wall acceleration in the former and centrifugal acceleration in the latter) is expected to increases in proportion to c^2. Contrasting figures 13(a, b) and 13(c, d), it becomes evident that the pressure gradients are mainly longitudinal for small c/U but vertical for large c/U with increasing vertical gradients as c/U increases. Our primary interest is not very large c/U, where our simulations (results not shown here) indicate that for $c/U \gg 1$ flow separation appears upstream of the crest resulting in the generation of a pressure thrust. An indication of the latter can already be discerned in figure 11 for larger c/U.

The effect of the different pressure distributions for low and high c/U on the drag can be seen more clearly in figure 14 which plots the mean pressure along the wall. The projection of the pressure force in the x-direction, f_x^p, is plotted in figure 15. For $c/U = 0.4$, the pressure force is mainly positive, serving as a form drag. At $c/U = 1.2$, the contributions on the two sides of the crest (and trough) almost cancel and consequently the net form drag is very small (figure 11).

Finally, we discuss the power, P_T, required for the propulsive motion of the wall. This consists of two parts. The first is the swimming power $P_S = \int \int p\, \mathrm{d}y_w/\mathrm{d}t\, \mathrm{d}x\, \mathrm{d}z$ required to produce the vertical oscillations of the travelling wave motion. The second is the power, $P_D = UF_d$, needed to overcome the drag force.

Figure 16 shows the variation of P_S, P_D and P_T as functions of c/U (see also table 1). At $c/U = 0$, $P_S = 0$ ($\mathrm{d}y_w/\mathrm{d}t = 0$). As c/U increases from zero, P_S first decreases, reaches a minimum (for c/U between 0 and 1) and then increases. The negative values of P_S at small c/U can be understood by examining the pressure distribution (figures 13 and 14): because of flow separation and reattachment, the pressure upstream/downstream of the crest (where $\mathrm{d}y_w/\mathrm{d}t$ negative/positive) is generally higher/lower, so that P_S is negative, i.e. the wall motion can be actuated by the flow and no power input is needed. (For negative c/U, the sign of $\mathrm{d}y_w/\mathrm{d}t$ is reversed
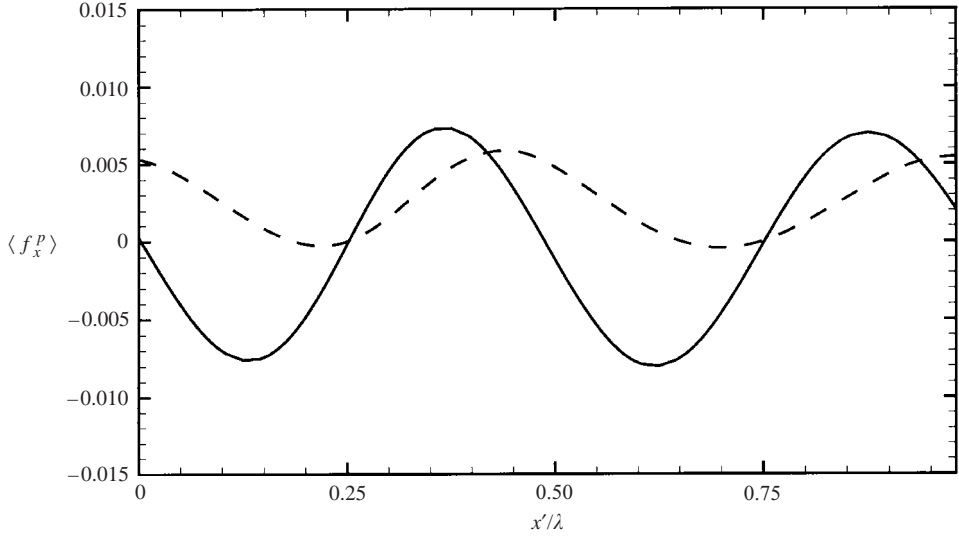
FIGURE 15. Distribution of x-component of pressure force acting on the wavy wall.
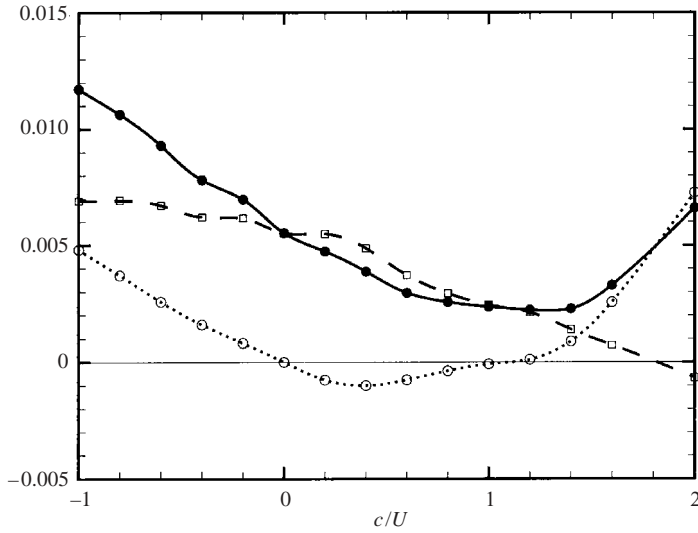$----$, $c/U = 0.4$; ———, $c/U = 1.2$.

FIGURE 16. Power required to propel a wavy wall for different c/U. $\cdot \circ \cdots \cdot$, swimming power P_S; $-\square--$, power required to overcome drag force P_D; ——•——, total power $P_T = P_S + P_D$.

but the pressure difference persists, so that P_S is positive.) As $c/U > 0$ increases, flow separation is weaker and the pressure gradient is mainly controlled by the wavy wall vertical motion. Eventually, at $c/U \approx 1$, the pressure becomes nearly symmetric (figures 13 and 14) and P_S again vanishes. P_S is positive for $c/U \gtrsim 1$. As expected, for $c/U \gg 1$, flow separation eventually occurs upstream of the crest, and P_S increases rapidly as c increases.

From figure 16 (and table 1), we see that P_D decreases monotonically as c/U increases, because of the similar decrease of F_d. For large c/U, P_D is negative,

indicating that the wavy surface is propelled by the thrust. This thrust is, however, at the expense of the swimming power P_S required to produce the wavy motion.

Combining the competing mechanisms P_S and P_D discussed above, the net power P_T as a function of c/U is concave upwards, with a minimum around $c/U = 1.2$. At this value of c/U, P_T is only 40% of the value at $c/U = 0$, so that there is a significant gain in net efficiency as a result of the travelling wave motion.

4. Discussion and conclusions

Direct numerical simulation is performed for turbulent flows over a smooth flexible wall undergoing streamwise travelling-wave transverse motions. The Reynolds number based on the free-stream velocity U and the travelling wave wavelength λ is $O(10^5)$, and the travelling wave amplitude a is given by $2\pi a/\lambda = 0.25$. By varying the ratio of the travelling wave phase speed c relative to the external stream velocity U, it is found that the wall oscillations can be optimized to achieve separation suppression and turbulence reduction, to create thrust, and to minimize net power input (for given U).

The problem can be considered as a simplified model of turbulent flow past an actively swimming fish. The modelled flow contains the interplay among four principal effects: the periodic interchange of favourable and adverse pressure gradients in the longitudinal direction; the wall-normal pressure gradients associated with the wall curvature; the wall-normal pressure gradients associated with the wall vertical motion; and, in a frame of reference moving with the phase speed, the non-zero wall tangential velocity and the reduction in the effective free-stream velocity. The former two are present in flow over a stationary wavy wall, while the latter two are unique to travelling wave motion ($c \neq 0$).

The overall flow pattern and dynamics depend strongly on the value of c/U. When the undulations are stationary ($c = 0$), there are regions of separated flow in the form of attached eddies. The features of this flow that we find are consistent with those from previous experimental and numerical studies. The travelling wave motion ($c \neq 0$) case is new. For upstream travelling wave motion ($c/U < 0$), the flow features are qualitatively similar to those for $c = 0$. The attached eddy flow persists, and intensifies with decreasing c/U, resulting in an increasingly greater drag force and the net energy needed for propulsion.

Our main interest is in downstream travelling wave motions ($c/U > 0$) where the flow is significantly altered. As c/U increases, the separation bubble moves away from the wall. This can be explained in terms of the positive vertical wall velocity at that location, and because of the negative wall tangential velocity relative to the fixed wall shape (in the frame moving at c). A more important effect is the weakening of the separation eddy with increasing c/U, eventually leading to its disappearance at $c/U \sim 1$. An explanation for this can be obtained by simply considering the effective inflow velocity, $U - c$, in a frame fixed to the wall shape. Another important effect of positive c/U is the dramatic reduction of the turbulence intensity and Reynolds stress. This turbulence suppression is non-uniform and is a function of the phase position relative to the moving wall. The main mechanism here is the reduction/elimination of the separation cell and the turbulence production associated with the separated-flow free shear layer.

In terms of the understanding of fish-like locomotion, the mean integrated forces and power are of primary concern. The drag force on the body is a sum of the pressure and frictional forces. It is found that, as c/U increases, the pressure force decreases

monotonically, becoming negative (thrust) at $c/U \sim 1$. The frictional force is always positive but smaller in magnitude, and is influenced by the presence/absence of flow reversal: a local maximum occurs at $c/U \sim 1$ where flow reversal is eliminated. Of equal importance is the swimming power required (for the vertical motion). By definition, this power is zero for $c = 0$ and for symmetric surface pressure relative to the crest (as in potential flow). For $c/U < 1$, the pressure minimum is shifted downstream relative to the crest due to flow separation, and this power is positive/negative for c/U negative/positive. Near $c/U = 1$, separation is eliminated and the swimming power again vanishes so that swimming power has a minimum for $0 < c/U < 1$. For very large (positive) c/U, the flow eventually separates upstream of the crest and the swimming power is positive. Of ultimate interest is the net power required for the locomotion, which is the sum of the swimming power and the power required to overcome the total drag. This sum yields a minimum for the net power required, which we find to be at $c/U \approx 1.2$. It is noteworthy that c/U around 1.2 is the value cited for travelling wave-like thunniform swimming motion of live fish in nature (e.g. Videler 1993; Videler & Hess 1984).

REFERENCES

Abrams, J. & Hanratty, T. J. 1985 Relaxation effects observed for turbulent flow over a wavy surface. *J. Fluid Mech.* **151**, 443–455.

Barrett, D. S., Triantafyllou, M. S., Yue, D. K. P., Grosenbaugh, M. A. & Wolfgang, M. J. 1999 Drag reduction in fish-like locomotion. *J. Fluid Mech.* **392**, 183–212.

Benjamin, T. B. 1959 Shearing flow over a wavy boundary. *J. Fluid Mech.* **6**, 161–205.

Bradshaw, P. 1969 The analogy between streamline curvature and buoyancy in turbulent shear flow. *J. Fluid Mech.* **36**, 177–191.

Buckles, J., Hanratty, T. J. & Adrian, R. J. 1984 Turbulent flow over large-amplitude wavy surfaces. *J. Fluid Mech.* **140**, 27–44.

Calhoun, R. J. & Street, R. L. 2001 Turbulent flow over a wavy surface: neutral case. *J. Geophys. Res.* **106**, 9277–9293.

Cherukat, P., Na, Y., Hanratty, T. J. & McLaughlin, J. B. 1998 Direct numerical simulation of a fully developed turbulent flow over a wavy wall. *Theoret. Comput. Fluid Dyn.* **11**, 109–134.

De Angelis, V., Lombardi, P. & Banerjee, S. 1997 Direct numerical simulation of turbulent flow over a wavy wall. *Phys. Fluids* **9**, 2429–2442.

Du, Y. Q. & Karniadakis, G. E. 2000 Suppressing wall turbulence by means of a transverse travelling wave. *Science* **288**, 1230–1234.

Du, Y. Q., Symeonidis, V. & Karniadakis, G. E. 2002 Drag reduction in wall-bounded turbulence via a transverse travelling wave. *J. Fluid Mech.* **457**, 1–34.

Eskinazi, S. & Yeh, H. 1956 An investigation on fully developed turbulent flows in a curved channel. *J. Aero. Sci.* **23**, 23–34.

Frederick, K. A. & Hanratty T. J. 1988 Velocity measurements for a turbulent nonseparated flow over solid waves. *Exps. Fluids* **6**, 477–486.

Görtler, H. 1940 On the three-dimensional instability of laminar boundary layers on concave walls. *Tech. Mem. Natl Adv. Comm. Aero. WA*, No. 1375 (1975).

Gray, J. 1936 Studies in animal locomotion. *J. Expl Biol.* **13**, 192–199.

Harlow, F. H. & Welch J. E. 1965 Numerical calculation of time-dependent viscous incompressible flow of fluid with free surface. *Phys. Fluids* **8**, 2182–2189.

Hudson, J. D., Dykhno, L. & Hanratty T. J. 1996 Turbulent production in flow over a wavy wall. *Exps. Fluids* **20**, 257–265.

Jeong, J. & Hussain, F. 1995 On the identification of a vortex. *J. Fluid Mech.* **285**, 69–94.

Kendall, J. M. 1970 The turbulent boundary layer over a wall with progressive surface waves. *J. Fluid Mech.* **41**, 259–281.

Kim, J., Moin P. & Moser R. 1987 Turbulent statistics in fully developed channel flow at low Reynolds number. *J. Fluid Mech.* **177**, 133–166.

Kuzan, J. D., Hanratty T. J. & Adrian, R. J. 1989 Turbulent flows with incipient separation over solid waves. *Exps. Fluids* **7**, 88–98.

Lighthill, M. J. 1962 Physical interpretation of the mathematical theory of wavy generation by wind. *J. Fluid Mech.* **14**, 385–398.

Longuet-Higgins, M. S. 1969 Action of a variable stress at the surface of water waves. *Phys. Fluids* **12**, 737–740.

Maass, C. & Schumann, U. 1994 Numerical simulation of turbulent flow over a wavy boundary. In *Direct and Large-Eddy Simulation* (ed. J.-P. Chollet, P. R. Voke & L. Kleiser), pp. 287–297. Kluwer.

Miles, J. W. 1957 On the generation of surface waves by shear flows. *J. Fluid Mech.* **3**, 185–204.

Miles, J. W. 1959 On the generation of surface waves by shear flows. Part 2. *J. Fluid Mech.* **6**, 568–582.

Prandtl, L. 1930 Vorträge auf dem Gebiet der Aerodynamik und verwandter Gebiete. *Gesammelte Abhandlungen Zur angewandten Mechanik, Hydround Aerodynamik, 1961*, Vol. 2, p. 778.

Rotta, J. C. 1967 Effect of streamwise wall curvature on compressible turbulent boundary layers. *Phys. Fluids* **10**, S174–S180.

So, R. M. C. & Mellor, G. L. 1973 Experiment on convex curvature effects in turbulent boundary layers. *J. Fluid Mech.* **60**, 43–62.

Taneda, S. & Tomonari, Y. 1974 An experiment on the flow around a waving plate. *J. Phys. Soc. Japan* **36**, 1683–1689.

Techet, A. H. 2001 Experimental visualization of the near-boundary hydrodynamics about fish-like swimming bodies. PhD thesis, Department of Ocean Engineering, MIT/WHOI.

Tokumaru, P. T. & Dimotakis, P. E. 1991 Rotary oscillation control of a cylinder wake. *J. Fluid Mech.* **224**, 77–90.

Triantafyllou, M. S., Triantafyllou, G. S. & Yue, D. K. P. 2000 Hydrodynamics of fishlike swimming. *Annu. Rev. Fluid Mech.* **32**, 33–53.

Videler, J. J. 1993 *Fish Swimming*. Chapman & Hall.

Videler, J. J. & Hess, F. 1984 Fast continuous swimming of two pelagic predators, saithe (pollachius virens) and mackerel (scomber scombrus): a kinematic analysis. *J. Expl Biol.* **109**, 209–228.

Wu. T. Y. 1961 Swimming of a waving plate. *J. Fluid Mech.* **10**, 321–344.

Zilker, D. P., Cook, G. W. & Hanratty, T. J. 1977 Influence of the amplitude of a solid wavy wall on a turbulent flow. Part 1. Non-separated flows. *J. Fluid Mech.* **82**, 29–51.

Zilker, D. P. & Hanratty, T. J. 1979 Influence of the amplitude of a solid wavy wall on a turbulent flow. Part 2. Separated flows. *J. Fluid Mech.* **90**, 257–271.